Edge Plasmons in Two-Component Electron Liquids in the Presence of Pseudomagnetic Fields

Alessandro Principi,[1] Mikhail I. Katsnelson,[1] and Giovanni Vignale[2]

[1]*Institute for Molecules and Materials, Radboud University, NL-6525 AJ Nijmegen, The Netherlands*
[2]*Department of Physics and Astronomy, University of Missouri, Columbia, Missouri 65211, USA*

We study the properties of edge plasmons in two-component electron liquids in the presence of pseudomagnetic fields, which have opposite signs for the two different electronic populations and therefore preserve the time-reversal symmetry. The physical realizations of such systems are many. We discuss the case of strained graphene, solving the problem with the Wiener-Hopf technique. We show (i) that two charged counterpropagating acoustic edge modes exist at the boundary and (ii) that, in the limit of large pseudomagnetic fields, each of them involves oscillations of only one of the two electronic components. We suggest that the edge pseudomagnetoplasmons of graphene can be used to selectively address the electrons of one specific valley, a feature relevant for the emerging field of valleytronics. Our solution highlights new features missing in previous (similar) results obtained with uncontrolled approximations, namely a logarithmic divergence of the plasmon velocity, and the absence of gapped edge modes inside the bulk-plasmon gap.

Introduction.—Nanoplasmonics, [1] which aims at compressing electromagnetic radiation to subwavelength scales by coupling it to matter waves, has recently experienced a strong revival [2–4] with the discovery of two-dimensional (2D) materials [5–15]. Atomically thin layers of van der Waals solids exhibit many remarkable and intriguing properties [11–13,16]; they allow to confine the radiation at a surface, coupling it with mobile electrons and forming surface-plasmon polaritons [2,15,17,18]. In this respect, graphene has attracted a lot of interest, especially for its record-high plasmon lifetimes [14,15]: plasmon losses have indeed represented so far the fundamental bottleneck for nanoplasmonic applications [19].

When a perpendicular magnetic field is applied to a 2D charged liquid, edge collective modes arise [20–22]. These "edge magnetoplasmons" have a linear low-energy dispersion and are decoupled from the (gapped) bulk modes [22]. Such modes are long lived thanks to the strong confinement at the edge and their quasi one dimensionality [23]. Fetter [20] calculated their dispersion in a two-dimensional electron gas (2DEG), even though its analytical solution exploited an uncontrolled approximation. Later he solved the same problem in the presence of nearby grounded metal plates by numerical methods [24]. Notably, edge magnetoplasmons can propagate in both directions along the edge; i.e., they are not chiral in a strict sense. However, chirality is still present since the "wrong-direction" plasmon is gapped, and its gap frequency increases with the magnetic field [20].

In many systems, electrons experience pseudomagnetic fields, whose main characteristic is to preserve the global time-reversal symmetry. This happens, e.g., in strained graphene [25–27]. Strain, modifying hopping parameters,

enters the low-energy Hamiltonian as a vector potential $A(r, t)$. The global time-reversal invariance is assured by the fact that A has opposite signs on the two inequivalent valleys (K and K') of the Brillouin zone. In spite of this, Landau quantization has been observed in strained samples and the effective magnetic field has been shown to reach values of hundreds of Tesla [28].

Naively, when doping is sufficiently high and intervalley scattering is neglected, one would expect the electrons of each valley to behave as a 2DEG subject to an effective magnetic field [Fig. 1(a)]. Each valley should exhibit two edge plasmons, one of which is gapped [Fig. 1(b)], with the direction of propagation of the acoustic plasmon
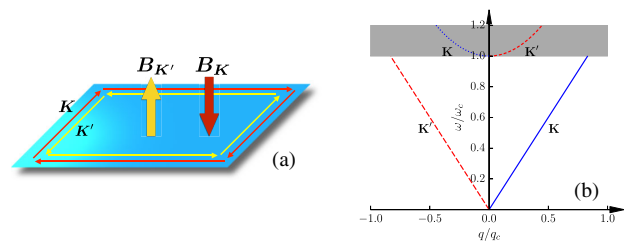

FIG. 1.   (a) Schematic view of the theoretical model: the two electronic components experience opposite pseudomagnetic fields. Two counterpropagating plasmons appear at the edge of the system, each of them mainly due to density oscillations in a specific valley. (b) Dispersion of edge collective modes in units of the cyclotron frequency ω_c, as a function of the momentum q measured in units of $q_c = (k_F \ell^2)^{-1}$ [$\ell = \sqrt{c/(eB)}$ is the magnetic length]. We set the filling factor $\nu = 1$ ($v_p \simeq 1.2 v_F$). Each electronic component, depending on the range of frequencies explored, can support up to two charged collective modes, one of which lives inside the gap of the particle-hole continuum (shaded region).

determined by the sign of the pseudomagnetic field in the given valley. Therefore, at low frequency one expects two counterpropagating edge magnetoplasmons to emerge, each due to density oscillations of one of the two electronic components. Unfortunately, the problem is not so simple: even neglecting direct scattering between them, the two valleys are always electrostatically coupled, and a density fluctuation in one of them invariably influences the electrons in the other. This fact makes the problem completely nontrivial and, since one of the two valleys is always off resonance (i.e., it experiences an effective magnetic field with the wrong sign), it could, in principle, destroy the collective modes. We find that the two counterpropagating acoustic edge plasmons survive, but that the valleys are not completely disentangled. Each collective mode stems indeed from the superposition of density oscillations in both valleys, and becomes "localized" in one of them only in the limit of large pseudomagnetic fields. We stress again that high field values are actually attainable in experiments.

In this Letter we solve the edge-plasmon problem in a two-component 2D electronic system subject to a pseudomagnetic field. We solve the full Wiener-Hopf problem [29] defined by constitutive equations and electrostatics, and we provide a comparison with an approximate solution obtained in a similar way as Fetter's one.

The model.—For the sake of definiteness we consider a strained graphene sheet that occupies the half plane $x < 0$, $z = 0$. We assume that the edge does not affect the low-energy physics of the system: electrons are described by the massless Dirac Hamiltonian [11–13]

$$\mathcal{H}_0 = v_F \sum_{\boldsymbol{k},\alpha,\beta} \hat{\psi}^{\dagger}_{\boldsymbol{k},\alpha} (\boldsymbol{k}+\boldsymbol{A}) \cdot \boldsymbol{\sigma}_{\alpha\beta} \hat{\psi}_{\boldsymbol{k},\beta}, \tag{1}$$

where $\hat{\psi}^{\dagger}_{\boldsymbol{k},\alpha}$ ($\hat{\psi}_{\boldsymbol{k},\alpha}$) creates (destroys) a particle with momentum $\boldsymbol{k}$ and pseudospin α, v_F is the Fermi velocity, $A_x = \xi\beta(u_{xx}-u_{yy})/a$, and $A_y = -2\xi\beta u_{xy}/a$ are the two components of the pseudomagnetic vector potential generated by the strain tensor $\boldsymbol{u}_{ij}(\boldsymbol{r})$ [here $\beta = -\partial \ln(t)/\partial \ln(a) \simeq 2$, $a = 1.4$ Å, and ξ is a numerical constant of order 1] [25–27]. We assume the strain field to be such that the pseudomagnetic field $\boldsymbol{\nabla} \times \boldsymbol{A} = \pm B\hat{z}$ is constant. The plus (minus) sign applies to electrons in valley $\boldsymbol{K}$ ($\boldsymbol{K'}$). Even though the strain field must have a trigonal symmetry to induce a constant B [25–27], we regard the edge as a straight line, assuming that its curvature is small. We neglect intervalley scattering, assume graphene to be in the Fermi-liquid regime [22], and describe the electronic transport by linearized hydrodynamic equations [30–32]. The electron densities in the two valleys satisfy separate continuity equations, i.e.,

$$\partial_t \delta n_K + n_0 \boldsymbol{\nabla} \cdot \boldsymbol{v}_K = 0,$$
$$\partial_t \delta n_{K'} + n_0 \boldsymbol{\nabla} \cdot \boldsymbol{v}_{K'} = 0, \tag{2}$$

where δn_K ($\delta n_{K'}$) is the nonequilibrium density fluctuation in valley K (K'), while n_0 is its equilibrium value. Hereafter we suppress space and time indices for brevity. The electron velocities $\boldsymbol{v}_K$ and $\boldsymbol{v}_{K'}$ obey the Navier-Stokes equations [22,33]

$$\partial_t \boldsymbol{v}_K + \omega_c \hat{z} \times \boldsymbol{v}_K + \frac{s^2}{n_0} \boldsymbol{\nabla} \delta n_K - \frac{e}{m} \boldsymbol{\nabla}\phi = 0,$$

$$\partial_t \boldsymbol{v}_{K'} - \omega_c \hat{z} \times \boldsymbol{v}_{K'} + \frac{s^2}{n_0} \boldsymbol{\nabla} \delta n_{K'} - \frac{e}{m} \boldsymbol{\nabla}\phi = 0, \tag{3}$$

where $m = \hbar k_F/v_F$ is the cyclotron mass (k_F is the Fermi momentum), $\omega_c = eB/(mc)$ is the classical cyclotron frequency, and $s = \sqrt{m^{-1}\partial P/\partial n} = v_F/\sqrt{2}$ [22]. Finally, the electrostatic potential is given by

$$\phi(\boldsymbol{r}) = e \int d^2 r' \frac{\delta n_K(\boldsymbol{r}') + \delta n_{K'}(\boldsymbol{r}')}{|\boldsymbol{r} - \boldsymbol{r}'|}. \tag{4}$$

Since the translational invariance along the $\hat{y}$ direction is not broken, all functions have a dependence of the form $e^{-i(\omega t - qy)}$. Equations (2)–(4) constitute a system of integrodifferential equations that can be solved using the Wiener-Hopf technique [29]. We calculate the sound velocity of the two counterpropagating edge pseudomagnetoplasmons. Furthermore, we show that in the limit $B \to \infty$ the two valleys decouple and each collective mode is due to density oscillations of only one of them.

Fetter [20] simplified the problem by introducing an approximation of Eq. (4), replacing it with

$$\partial_x^2 \phi(x) - 2q^2 \phi(x) = 4\pi e|q|[\delta n_K(x) + \delta n_{K'}(x)]. \tag{5}$$

The big advantage of Eq. (5) is that, while leaving intact the first two moments of the interaction potential integrated across the edge, it allows us to study a system of ordinary linear differential equations. However, effects that depend on the long range of the interaction *along* the edge are in this way lost. Note indeed that the asymptotic behavior of Eq. (5) in the limit $q \to 0$ is completely different from that of the Fourier transform of Eq. (4). Below, we compare our exact results with those obtained with the approximation (5). We stress that the solution obtained with the Wiener-Hopf method is not just an incremental improvement of Fetter's result, but reveals features missing in the approximate result: namely, (i) the logarithmic divergence of the plasmon velocity at small momenta due to the long-range nature of the Coulomb interaction [21], and (ii) the absence of gapped modes with energy below $\hbar\omega_c$. Details of the calculation in the approximate model, which closely parallels Fetter's derivation [20], are given in the Supplemental Material [34].

The Wiener-Hopf solution.—To solve the problem posed by Eqs. (2)–(4), we first introduce $n_{\mathrm{sum(diff)}}(x) \equiv \delta n_K(x) \pm \delta n_{K'}(x)$. The resulting equation for $n_{\mathrm{diff}}(x)$ is independent of $\phi(x)$, and its solution reads $n_{\mathrm{diff}}(x) = \bar{n}_{\mathrm{diff}} e^{\kappa_- x}$, where $\kappa_- = \sqrt{q^2 + s^{-2}(\omega_c^2 - \omega^2)}$.
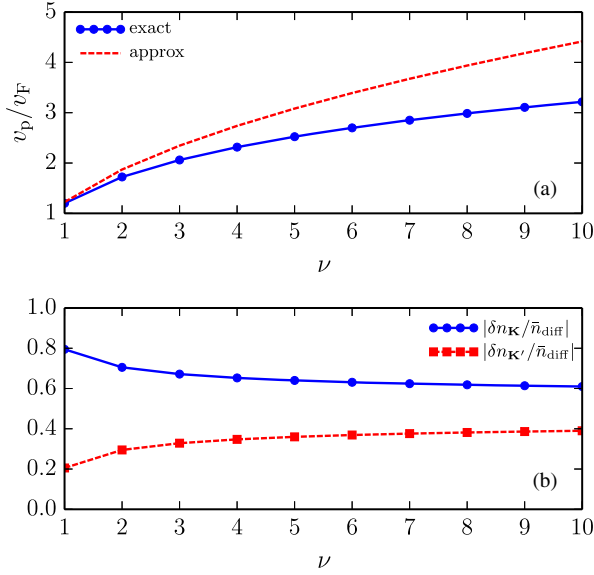
FIG. 2.   (a) Sound velocity of the acoustic edge pseudomagne-
toplasmon $v_p = \omega_p(q)/q$ in units of the Fermi velocity, plotted
as a function of the filling factor ν. The dots represent the Wiener-
Hopf result, while the dashed line is the approximate solution of
Eq. (14). We cut off the logarithmic divergence of v_p by setting
$\bar{q} = 0.01$. (b) Degree of valley polarization of the right-moving
edge pseudomagnetoplasmon, given by $|\delta n_K/\bar{n}_{\text{diff}}| = (v_p + s)/
(2v_p)$ and $|\delta n_{K'}/\bar{n}_{\text{diff}}| = (v_p - s)/(2v_p)$. Note that at large
magnetic field ($\nu = 1$), 80% of the contribution to density
oscillations comes from electrons in valley K, and only 20%
from those living around the K' point. For the left-moving edge
plasmon an analogous figure can be drawn with valleys K and K'
interchanged.

$\bar{n}_{\text{diff}}$ is a constant to be determined from the boundary
conditions. Plugging this solution back into Eqs. (2)–(4),
and taking their one-sided Fourier transform [29], we find

$$n_{\text{sum}}(k) = \frac{\frac{2en_0}{ms^2}(k^2 + q^2)\phi(k) + [ik + \frac{q^2}{\kappa_-}\frac{\omega_c^2}{\omega^2}]\bar{\Xi}}{k^2 + \kappa_-^2}, \quad (6a)$$

$$\bar{n}_{\text{diff}} = \frac{q}{\kappa_-}\frac{\omega_c}{\omega}\bar{\Xi}. \quad (6b)$$

Here we used the fact that $v_{K,x}(0) = v_{K',x}(0) = 0$, and we
defined $\bar{\Xi} \equiv n_{\text{sum}}(0) - 2en_0\phi(0)/(ms^2)$. We extend k to
the whole complex plane, denoting with the subscript "+"
("−") functions analytic in the upper (lower) half. The
functions $n_{\text{sum}}(k)$ and $\phi(k)$ in Eq. (6a) are, by construction,
analytic for $\Im m(k) \geq 0$ [29]. We therefore rename $\phi(k) \to
\phi_+(k)$ and $n_{\text{sum}}(k) \to n_+(k)$. Analyticity requires the
numerator of Eq. (6a) to vanish for $k = i\kappa_-$: we use this
condition below to determine the plasmon dispersion.
Taking the double-sided Fourier transform of Eq. (4),
noting that the left-hand side is $\phi_+(k) + \phi_-(k)$, and
combining it with Eq. (6a) we get

$$(k^2 + \kappa_-^2)G(k)\phi_+(k) + (k^2 + \kappa_-^2)\phi_-(k) = 2\pi e\bar{\Xi}F(k), \quad (7)$$

where $G(k) \equiv 1 + 2\alpha\sqrt{k^2 + q^2}/(k^2 + \kappa_-^2)$, $F(k) = -[ik +
q^2\omega_c^2/(\kappa_-\omega^2)]/\sqrt{k^2 + q^2}$, and $\alpha = 2\pi e^2 n_0/(ms^2)$.
Equation (7) can be solved with the Wiener-Hopf tech-
nique. Using a well-known theorem of complex analysis
[29], we rewrite $G(k) = G_+(k)/G_-(k)$, where ($\eta \to 0^+$)

$$G_\pm(k) = \exp\left[\int_{-\infty\mp i\eta}^{\infty\mp i\eta} \frac{dz}{2\pi i}\frac{\ln G(z)}{z - k}\right]. \quad (8)$$

The function $G_+(k)$ [$G_-(k)$] is analytic in the upper (lower)
half of the complex plane. Equation (7) then becomes

$$G_+(k)\phi_+(k) + G_-(k)\phi_-(k) = 2\pi e\bar{\Xi}F(k)\frac{G_-(k)}{k^2 + \kappa_-^2}. \quad (9)$$

The term on the right-hand side of Eq. (9) can be rewritten
as $F(k)G_-(k)/(k^2 + \kappa_-^2) = F_+(k) + F_-(k)$ [29], where
$F_+(k)$ [$F_-(k)$] is analytic in the upper (lower) half of
the complex plane, and reads

$$F_\pm(k) = \pm\int_{-\infty\mp i\eta}^{\infty\mp i\eta} \frac{dz}{2\pi i}\frac{F(z)}{z - k}\frac{G_-(z)}{z^2 + \kappa_-^2}. \quad (10)$$

Equation (9) now reads

$$G_+(k)\phi_+(k) - 2\pi eF_+(k)\bar{\Xi} = 2\pi eF_-(k)\bar{\Xi} - G_-(k)\phi_-(k). \quad (11)$$

Since the left-hand side is analytic for $\Im m(k) \geq 0$ and the
right-hand side is analytic for $\Im m(k) \leq 0$, together they
define a function analytic in the whole complex plane.
Moreover, both sides of Eq. (11) vanish in the limit
$|k| \to \infty$. Therefore [29] they must be separately equal
to 0, and $\phi_+(k) = 2\pi e\bar{\Xi}F_+(k)/G_+(k)$. Equation (6a) now
reads

$$n_+(k) = \left[2\alpha(k^2 + q^2)\frac{F_+(k)}{G_+(k)} + ik + \frac{q^2}{\kappa_-}\frac{\omega_c^2}{\omega^2}\right]\frac{\bar{\Xi}}{k^2 + \kappa_-^2}. \quad (12)$$

Since $n_+(k)$ is, by definition, analytic for $\Im m(k) > 0$, the
square brackets in Eq. (12) must vanish for $k = i\kappa_-$ in order
to cancel the pole in the denominator. Performing the
integrals (8) and (10), setting $\omega_p(q) = v_pq$, and taking the
limit $q \to 0$, from the square brackets in Eq. (12) we get
$s^2/v_p^2 - 1 = 2\bar{\alpha}f/g$, where

$$g = \exp\left[\frac{2\bar{\alpha}}{\pi}\int_0^\infty dx \frac{x^2+1}{(x^2-1)^2+4\bar{\alpha}^2 x^2}\ln\left(\frac{1+x}{2}\right)\right],$$

$$f = \frac{1}{\pi}\mathcal{P}\int_{\bar{q}}^\infty \frac{dy}{y+1}\left(\frac{s^2}{v_p^2}+y\right)\frac{y^{-1}}{y^2-1}$$

$$\times \exp\left[-\frac{2\bar{\alpha}}{\pi}\int_0^\infty dx \frac{(x^2+1)\ln(\frac{y+x}{y+1})}{(x^2-1)^2+4\bar{\alpha}^2 x^2}\right]. \quad (13)$$

Here $\bar{q} \equiv sq/\omega_c$ and $\bar{\alpha} \equiv s\alpha/\omega_c = \sqrt{2}N_F\alpha_{ee}(\nu-1/2)$, where N_F is the number of residual fermion flavors, $\alpha_{ee} = e^2/(\hbar v_F)$ the dimensionless coupling constant, and ν is the filling factor. In the presence of unscreened electron-electron interactions the integral on the second line is infrared divergent in the limit $\bar{q} \to 0$. The edge pseudo-magnetoplasmon velocity therefore diverges as $v_p^2 \to -2s^2\bar{\alpha}\ln(\bar{\alpha}\bar{q})/\pi$ (when $\bar{\alpha} \ll 1$) [35]. From this we extract the length scale $\lambda \equiv \bar{\alpha}s/\omega_c = 2\pi e^2 n_0/(m\omega_c^2)$, which is the typical size of the boundary layer [21]. Solving the problem in a similar way as Fetter's magnetoplasmon [34], i.e., replacing Eq. (4) with Eq. (5), we find

$$v_{p,\text{approx}} = s\sqrt{1+2\sqrt{2}\frac{2\pi e^2 n_0}{ms\omega_c}}. \quad (14)$$

A comparison between v_p and the approximate result of Eq. (14) is given in Fig. 2(a). In this plot we set $\bar{q} = 0.01$.

Since the problem is symmetric for $q \to -q$, at any given frequency two counterpropagating plasmons can be excited. Once a plasmon is excited, the two electronic components oscillate with opposite phases [34]. Therefore $|n_{\text{diff}}| > |n_{\text{sum}}|$. Hence, to display the degree of valley polarization we consider $|\delta n_K/n_{\text{diff}}|$ and $|\delta n_{K'}/n_{\text{diff}}|$. For weak pseudomagnetic fields the two are identical, and both valleys oscillate simultaneously. However, in the limit $B \to \infty$ one of the them is completely "frozen" and oscillations involve only the other valley. In this case, e.g., $|\delta n_K/n_{\text{diff}}| \simeq 1$ and $|\delta n_{K'}/n_{\text{diff}}| \simeq 0$. We derive an explicit expression for these two quantities. First, when $\omega = \omega_p(q)$, $\bar{n}_{\text{diff}} = s\bar{\Xi}/v_p$ [see Eq. (6b)]. The value of $n_{\text{sum}}(x=0)$ is obtained by taking the Fourier transform of Eq. (12) in the limit $x \to 0^-$ [34]. The resulting expressions are fairly simple, but their numerical evaluation turns out to be quite challenging. We therefore resort to the approximate model, which gives $n_{\text{sum}}(0) = s^2\bar{\Xi}/v_p^2$, in very good agreement with the result obtained by the Wiener-Hopf technique (when v_p is calculated with this method). Using the approximate expression, $|\delta n_K/n_{\text{diff}}| = (v_p+s)/(2v_p)$ and $|\delta n_{K'}/\bar{n}_{\text{diff}}| = (v_p-s)/(2v_p)$. In Fig. 2(b) we plot the two functions for the right-propagating mode. At $\nu = 1$ 80% (20%) of the contribution comes from electrons of valley K (K').

It is also possible to show that no other mode lives inside the bulk-plasmon gap. Such a mode should have a zero-momentum frequency smaller than ω_c. The plasmon equation for gapped modes is obtained as before by considering the term in the square brackets in Eq. (12) and setting $k = i\kappa_-$ and $\omega = \omega_c\Delta$, with $0 < \Delta < 1$. In the limit $q \to 0$ the resulting equations are identical to those obtained before, when these are evaluated in the limit $v_p \to \infty$ and $\bar{\alpha} = s\alpha/(\omega_c\sqrt{1-\Delta^2})$. The plasmon equation is therefore a function of only $\bar{\alpha}$, and has no solution unless $\bar{\alpha} \to \infty$ (i.e., for $\Delta = 1$). Therefore the gapped mode has a minimum energy equal to $\hbar\omega_c$.

Finally, intervalley scattering introduces a mechanism of nonconservation of the valley density. Equations (2) are therefore amended by adding the terms $(\delta n_K - \delta n_{K'})/\tau_I$ with opposite signs in the two equations. Extending the Wiener-Hopf calculation in the presence of the intervalley scattering we find that, in the limit of $\tau_I^{-1} \ll cq$, the pseudomagnetoplasmon dispersion becomes $\omega_p(q) = v_p q + i/(2\tau_I)$ [34].

Conclusions.—In this Letter we have discussed the problem of collective modes confined at the boundaries of a two-component 2D system subject to a pseudomagnetic field that preserves the time-reversal symmetry [25–27,36,37]. This property is ensured by the fact that it has opposite signs for the two different electron populations. We have shown that (i) two counterpropagating acoustic plasmons live at the edge of the system, and that (ii) in the limit of large pseudomagnetic field the excited plasmon involves only density oscillations of one of the two electronic components, while the other is frozen.

In graphene, edge modes induced by shear strain deformations [25–27] are valley polarized. They can therefore be used to selectively excite electrons in one of the two valleys by, e.g., optical means, by carefully choosing the energy and wave vector of the imparted external perturbation. This fact, similar to the valley-selective circular dichroism of transition metal dichalcogenides [38], has a direct impact on the emerging field of valleytronics [38–40]. Furthermore, since the edge-plasmon velocity depends on the strain field, it is possible to draw an analogy with the propagation of light in media with different refractive indexes, and imagine inducing focusing, antifocusing, and interference between collective modes by means of a properly chosen strain pattern [25–28].

Our edge pseudomagnetoplasmons are conceptually different from the edge "Berry plasmons" recently introduced in Ref. [41]. The latter are driven by a pseudomagnetic field in momentum space (Berry curvature) whereas our valley-selective pseudomagnetic field acts in real space, therefore opening a gap in the spectrum of the modes propagating in the wrong direction. No such gap is present in the spectrum of Berry plasmons.

Being unidirectional as well as valley polarized (in the large-strain limit), edge plasmons are expected to be long-lived excitations only weakly affected by smooth charge inhomogeneities. Once launched by, e.g., an s-SNOM setup

[17,18,42] or fast electric pulses applied to an electrode [23,43], they can be detected in real-time measurements far away from the injection point [23,43]. Furthermore, the combination of a *real* magnetic field with strain creates an asymmetry in the velocity of the two counterpropagating plasmons. The observed difference between plasmon velocities in opposite directions can be compared with theoretical predictions to reveal the valley-polarized nature of pseudomagnetoplasmons. Finally, edge pseudomagnetoplasmons in graphene nanodisk arrays can be revealed in IR-THz optical absorption measurements from the splitting of the low-energy peak in the presence of both strain and magnetic field [44].

A more exotic testing ground for these ideas is given by electrons traveling in a Skyrmion lattice [36,37]. The complex, topological magnetic structure of the Skyrmions is responsible for the emergence of an "effective electrodynamics," under which electrons experience a spin-dependent pseudomagnetic field similar to the one described in this Letter, with the spin index replacing the valley index. In this case, our theory predicts the existence of counterpropagating spin-polarized acoustic plasmons, which could be exploited for spintronics applications [45–47]. The anomalous Hall effect arising from the net magnetic moment of the Skyrmion is expected to be a minor correction to the main effect.

[1] M. I. Stockman, Opt. Express **19,** 22029 (2011).
[2] A. N. Grigorenko, M. Polini, and K. S. Novoselov, Nat. Photonics **6,** 749 (2012).
[3] A. G. Brolo, Nat. Photonics **6,** 709 (2012).
[4] M. L. Brongersma, N. J. Halas, and P. Nordlander, Nat. Nanotechnol. **10,** 25 (2015).
[5] K. S. Novoselov, A. K. Geim, S. V. Morozov, D. Jiang, M. I. Katsnelson, I. V. Grigorieva, S. V. Dubonos, and A. A. Firsov, Nature (London) **438,** 197 (2005).
[6] K. S. Novoselov, D. Jiang, F. Schedin, T. J. Booth, V. V. Khotkevich, S. V. Morozov, and A. K. Geim, Proc. Natl. Acad. Sci. U.S.A. **102,** 10451 (2005).
[7] A. K. Geim and K. S. Novoselov, Nat. Mater. **6,** 183 (2007).
[8] A. K. Geim and I. V. Grigorieva, Nature (London) **499,** 419 (2013).
[9] A. V. Kretinin *et al.*, Nano Lett. **14,** 3270 (2014).
[10] J. D. Caldwell and K. S. Novoselov, Nat. Mater. **14,** 364 (2015).
[11] A. H. Castro Neto, F. Guinea, N. M. R. Peres, K. S. Novoselov, and A. K. Geim, Rev. Mod. Phys. **81,** 109 (2009).
[12] S. Das Sarma, S. Adam, E. H. Hwang, and E. Rossi, Rev. Mod. Phys. **83,** 407 (2011).
[13] V. N. Kotov, B. Uchoa, V. M. Pereira, F. Guinea, and A. H. Castro Neto, Rev. Mod. Phys. **84,** 1067 (2012).
[14] A. Principi, M. Carrega, M. B. Lundeberg, A. Woessner, F. H. L. Koppens, G. Vignale, and M. Polini, Phys. Rev. B **90,** 165408 (2014).
[15] A. Woessner *et al.*, Nat. Mater. **14,** 421 (2015).
[16] K. F. Mak and J. Shan, Nat. Photonics **10,** 216 (2016).
[17] J. Chen *et al.*, Nature (London) **487,** 77 (2012).
[18] Z. Fei *et al.*, Nature (London) **487,** 82 (2012).
[19] J. B. Khurgin, Nat. Nanotechnol. **10,** 2 (2015).
[20] A. L. Fetter, Phys. Rev. B **32,** 7676 (1985).
[21] V. A. Volkov and S. A. Mikhailov, J. Exp. Theor. Phys. Lett. **42,** 556 (1985).
[22] G. F. Giuliani and G. Vignale, *Quantum Theory of the Electron Liquid* (Cambridge University Press, Cambridge, 2005).
[23] N. Kumada, P. Roulleau, B. Roche, M. Hashisaka, H. Hibino, I. Petković, and D. C. Glattli, Phys. Rev. Lett. **113,** 266601 (2014).
[24] A. L. Fetter, Phys. Rev. B **33,** 3717 (1986).
[25] F. Guinea, M. I. Katsnelson, and A. K. Geim, Nat. Phys. **6,** 30 (2010).
[26] F. Guinea, A. K. Geim, M. I. Katsnelson, and K. S. Novoselov, Phys. Rev. B **81,** 035408 (2010).
[27] M. A. H. Vozmediano, M. I. Katsnelson, and F. Guinea, Phys. Rep. **496,** 109 (2010).
[28] N. Levy, S. A. Burke, K. L. Meaker, M. Panlasigui, A. Zettl, F. Guinea, A. H. Castro Neto, and M. F. Crommie, Science **329,** 544 (2010).
[29] B. Noble, *Methods Based on the Wiener-Hopf Technique* (Pergamon Press, London, 1958).
[30] A. Principi, G. Vignale, M. Carrega, and M. Polini, Phys. Rev. B **93,** 125410 (2016).
[31] D. A. Bandurin *et al.*, Science **351,** 1055 (2016).
[32] J. Crossno *et al.*, Science **351,** 1058 (2016).
[33] L. D. Landau and E. M. Lifshitz, *Course of Theoretical Physics: Fluid Mechanics* (Pergamon Press, Oxford, 1987).
[34] See the Supplemental Material at http://link.aps.org/supplemental/10.1103/PhysRevLett.117.196803, for details of the Wiener-Hopf derivation and of the approximate solution in the manner of Fetter.
[35] Since the system is time-reversal invariant, the dispersion of edge pseudomagnetoplasmons ($\omega_p \sim q\sqrt{|\ln(q)|}$) is significantly different from that of standard edge magnetoplasmons ($\omega_p \sim q|\ln(q)|$), and closely resembles the plasmon dispersion in time-reversal invariant (i.e., nonchiral) Luttinger liquids.
[36] T. Schulz, R. Ritz, A. Bauer, M. Halder, M. Wagner, C. Franz, C. Pfleiderer, K. Everschor, M. Garst, and A. Rosch, Nat. Phys. **8,** 301 (2012).
[37] P. Bruno, V. K. Dugaev, and M. Taillefumier, Phys. Rev. Lett. **93,** 096806 (2004).
[38] H. Zeng, J. Dai, W. Yao, D. Xiao, and X. Cui, Nat. Nanotechnol. **7,** 490 (2012).
[39] A. Rycerz, J. Tworzydło, and C. W. J. Beenakker, Nat. Phys. **3,** 172 (2007).
[40] J. Kim, X. Hong, C. Jin, S.-F. Shi, C.-Y. S. Chang, M.-H. Chiu, L.-J. Li, and F. Wang, Science **346,** 1205 (2014).
[41] J. C. W. Song and M. S. Rudner, Proc. Natl. Acad. Sci. U.S.A. **113,** 4658 (2016).

[42] A. Y. Nikitin *et al.*, Nat. Photonics **10**, 239 (2016).

[43] R. C. Ashoori, H. L. Stormer, L. N. Pfeiffer, K. W. Baldwin, and K. West, Phys. Rev. B **45**, 3894(R) (1992).

[44] H. Yan, Z. Li, X. Li, W. Zhu, P. Avouris, and F. Xia, Nano Lett. **12**, 3766 (2012).

[45] J. Sinova, D. Culcer, Q. Niu, N. A. Sinitsyn, T. Jungwirth, and A. H. MacDonald, Phys. Rev. Lett. **92**, 126603 (2004).

[46] E. G. Mishchenko, A. V. Shytov, and B. I. Halperin, Phys. Rev. Lett. **93**, 226602 (2004).

[47] J.-I. Inoue, G. E. W. Bauer, and L. W. Molenkamp, Phys. Rev. B **70**, 041303(R) (2004).